



# Mechanistic insights into marine boundary layer nucleation: synergistic interactions of typical sulfur, iodine, and nitrogen precursors

Jing Li<sup>1</sup>, An Ning<sup>1,\*</sup>, Ling Liu<sup>1</sup>, Xiucong Deng<sup>1</sup>, and Xiuhui Zhang<sup>1,\*</sup>

<sup>1</sup>State Key Laboratory of Environment Characteristics and Effects for Near-space, Key Laboratory of Cluster Science, Ministry of Education of China, School of Chemistry and Chemical Engineering, Beijing Institute of Technology, Beijing, 100081, China

Correspondence to: A. Ning (anning@bit.edu.cn) and X. H. Zhang (zhangxiuhui@bit.edu.cn)

Abstract. Marine new particles have significant impacts on the global atmosphere, yet the key nucleation process underlying their formation remains highly unclear. Given the coexistence of multiple marine nucleating agents, here we explored how typical sulfur-, iodine-, and nitrogen-bearing chemicals, i.e., methanesulfonic acid (MSA), iodic acid (IA), and dimethylamine (DMA), synergistically interact to drive particle nucleation at the molecular level, by high-level quantum chemical calculations and cluster dynamics simulations. The results show that IA, MSA, and DMA can form stable pre-nucleation clusters via intermolecular hydrogen bonding and halogen bonding, with acid-base reactions occurring during their clustering, yielding ion pair formation. The proposed IA–MSA–DMA ternary nucleation is thermodynamically more favorable in regions rich in sulfur and nitrogen but poor in iodine. The cluster formation rate of IA–MSA–DMA ternary system is notably higher than that of any corresponding binary nucleation, showing a synergistic enhancement on rate of 4–8 orders of magnitude. Moreover, this rate even exceeds that of the well-established efficient iodine oxoacids nucleation under sulfur-rich conditions. In polar coastal regions such as Aboa and Marambio, the simulated rates of IA–MSA–DMA nucleation better agree with field measurements compared with the established IA–DMA nucleation. Accordingly, the proposed IA–MSA–DMA nucleation mechanism is expected to be important in the marine boundary layer, helping to explain the missing sources of iodic acid particles, especially in cold polar marine regions. Incorporating this mechanism into the atmospheric modeling can potentially improve aerosol formation simulations and refine climate predictions.

#### 1 Introduction

20

Marine aerosols represent the largest aerosol system on Earth, influencing global radiative balance and climate change (O'Dowd and Leeuw, 2007; Zhang et al., 2012). Notably, aerosols are the primary source of uncertainty in climate forcing (Gettelman and Kahn, 2025). And aerosols originate primarily from new particle formation (NPF), initiated by nucleation processes that involves the gas-to-particle transition—a critical yet elusive stage (Kulmala et al., 2013). Field studies have



30

40



shown that marine NPF events are closely linked to iodine-bearing precursors, with iodic acid (HIO<sub>3</sub>, IA) playing a key role in driving nucleation (Sipilä et al., 2016; Baccarini et al., 2020; Beck et al., 2021; He et al., 2021; He et al., 2023).

Although IA is abundant and widespread, its self-nucleation is insufficient to explain the fast nucleation observed (Ning et al., 2022a; Ma et al., 2023). Even with the effective stabilization by iodous acid (HIO<sub>2</sub>), the predicted nucleation rates cannot fully account for the high values measured in previous experiments (Engsvang and Elm, 2025). As an acidic precursor, IA is readily stabilized by atmospheric base such as ammonia (NH<sub>3</sub>) and amines (e.g., dimethylamine, DMA) (Rong et al., 2020; Xia et al., 2020; Ning et al., 2022b; Ma et al., 2023; Li et al., 2024) via acid-base reactions. Among these bases, DMA stabilizes IA more efficiently—by 1000-fold compared to NH<sub>3</sub> (Ning et al., 2022b). Accordingly, when NH<sub>3</sub> and DMA coexist, IA–DMA clusters play a more important role in nucleation under ambient conditions of boundary layer (Li et al., 2024). A recent study has also confirmed that IA–amine nucleation is efficient enough to be comparable to the well-established sulfuric acid–amine nucleation, provided that IA exceeds sulfuric acid by a factor of 10 (Engsvang and Elm, 2025). However, IA–DMA mechanism overlooks the roles and effects of other effective nucleation precursors, failing to capture the complexity of real atmospheric scenarios.

Alongside the aforementioned efficient iodine (IA) and nitrogen (DMA) precursors, historically, sulfur-containing compounds have also been regarded as vital nucleation agents over oceans, primarily the oxidation product of dimethyl sulfide (DMS) (Hodshire et al., 2019; Hoffmann et al., 2016). As the typical oxidation product of DMS, methanesulfonic acid (MSA) is ubiquitous in marine atmospheres, often present at considerable concentrations (Chen et al., 2018; Dal Maso et al., 2002; Yan et al., 2019; Eisele and Tanner, 1993), and existing observational data may even underestimate its true levels (Yan et al., 2019). More importantly, MSA shows effective nucleation potential, even comparable to that of H<sub>2</sub>SO<sub>4</sub> (Liu et al., 2022; Perraud et al., 2015; Dawson et al., 2012), and can individually bind with IA and DMA to form binary clusters, respectively (Ning et al., 2022a; Chen et al., 2016; Chen and Finlayson-Pitts, 2017). Nevertheless, theoretical studies suggest that electrically neutral clusters consisting solely of MSA (as the clustering acid) are unlikely to form and grow under realistic atmospheric conditions (Elm, 2021). Moreover, field observations indicate that MSA frequently coexists with IA and DMA in the marine atmosphere, and all three species are simultaneously detected in aerosol particle (Salignat et al., 2024). Collectively, the evidence points to the coexistence and potential interactions of these typical marine sulfur-(MSA), iodine-(IA), and nitrogen-(DMA) precursors, implying their possibility to jointly participate in particle nucleation. However, whether these three precursors exhibit synergistic effects, as well as the underlying molecular mechanisms and their atmospheric implications, remains unclear. Thus, elucidating the IA-MSA-DMA ternary nucleation process is crucial for a deeper understanding of the underlying origins of marine NPF events.

Herein, we investigated the IA-MSA-DMA ternary nucleation system (denoted as  $(IA)_x(MSA)_y(DMA)_z$ , where  $x + y + z \le 6$  and  $x + y \ge z$ ) at the molecular level using quantum chemical (QC) calculations and cluster dynamics simulations. QC calculations and wavefunction analyses were performed to clarify the physicochemical nature of clustering, while nucleation rates under varying atmospheric conditions were calculated to reveal nucleation dynamics. By comparing nucleation simulations with field observations (or other well-established nucleation systems), we assess and quantify the importance of





IA-MSA-DMA nucleation mechanism. Furthermore, by analyzing the nucleation pathway under different latitudinal marine conditions, we quantify the contribution of IA-MSA-DMA ternary nucleation to particle formation.

#### 65 2 Methods

## 2.1 Quantum Chemistry Calculations

In this study, a multistep conformation search was employed to identify the lowest-energy structures of  $(IA)_x(MSA)_y(DMA)_z(1 \le x + y + z \le 6, x + y \ge z)$  clusters. A detailed description of the methodology is provided in the Supporting Information (SI). The initial structures of pure IA clusters, as well as binary IA–MSA, IA–DMA, and MSA–DMA clusters, were adopted from the previous studies (Rong et al., 2020; Ning et al., 2022a; Ning et al., 2022b; Ning and Zhang, 2022). All lowest-energy structures of IA–MSA–DMA ternary cluster were further optimized using the Gaussian 09 program (Frisch et al., 2009) at the  $\omega$ B97X-D/6-311++G(3df,3pd) (for C, H, O, N, and S atoms) + aug-cc-pVTZ-PP (for I atom) level of theory (Francl et al., 1982; Peterson et al., 2003). Subsequent single-point energy calculations were carried out using the ORCA 5.0 software (Neese, 2012) at the DLPNO-CCSD(T)/aug-cc-pVTZ (for C, H, O, N, and S atoms) + aug-cc-pVTZ-PP (for I atom) level of theory, with the TightPNO and TightSCF criteria applied to ensure high-accuracy electronic energies. Given the significant impact of spin-orbit coupling (SOC) on energy calculations for heavy elements like iodine (Verstraete et al., 2008; Mohd Zaki et al., 2023; Engsvang et al., 2024), we quantitatively evaluated SOC effects using the Gaussian 16 program (Frisch et al., 2016) at the  $\omega$ B97X-D/6-311++G(3df,3pd) (for C, H, O, N, and S atoms) + dhf-TZVP-2c (for I atom) level of theory (Chan and Yim, 2013; Kuhn and Weigend, 2015; Sarr et al., 2021; Holzer et al., 2022). Gibbs free energies ( $\Delta$ G<sub>ref</sub>, kcal mol<sup>-1</sup>) of the IA–MSA–DMA clusters under standard pressure were calculated using Eq. (1):

$$\Delta G_{\text{ref}} = \Delta G_{\text{thermal}}^{\omega B97X-D} + \Delta E_{\text{DLPNO-CCSD(T)}} + \Delta E_{\text{SOC}}, \tag{1}$$

where  $\Delta G_{\text{thermal}}^{\text{oB97X-D}}$  and  $\Delta E_{\text{DLPNO-CCSD(T)}}$  represent the thermal and electronic contributions to the Gibbs free energy, respectively.  $\Delta E_{\text{SOC}}$  denotes the relativistic correction from SOC for iodine-containing clusters. Thermal corrections ( $\Delta G_{\text{thermal}}^{\text{oB97X-D}}$ ) across the temperature range of 258 – 298 K were obtained using Shermo 2.0 software (Lu and Chen, 2021). Final Gibbs free energies are summarized in Table S1 of the SI. To account for the influence of precursor concentrations, the  $\Delta G_{\text{ref}}$  was further converted to the concentration-dependent Gibbs free energy ( $\Delta G$ ) using Eq. (2):

$$\Delta G(P_1, P_2, \dots, P_n) = \Delta G_{\text{ref}} - k_B T \sum_{i=1}^n N_i \ln \left( \frac{P_i}{P_{\text{ref}}} \right), \tag{2}$$

where  $P_{\text{ref}}$  is the reference pressure (1 atm),  $k_{\text{B}}$  is the Boltzman constant, T is the temperature,  $N_i$  is the number of molecules i in the cluster, and  $P_i$  is the partial pressure of vapor i.





## 90 2.2 Wavefunction Analysis

The stability of clusters is largely determined by intermolecular forces between constituent molecules. To gain deeper insight into these interactions within the IA-MSA-DMA clusters, wavefunction-based analyses were performed using the Multiwfn 3.7 program (Lu and Chen, 2012). Specifically, the electrostatic potential (ESP) was projected onto the molecular van der Waals (vdW) surface to identify favorable interaction regions of the nucleating species, namely IA, MSA, and DMA.

## 95 2.3 Atmospheric Clusters Dynamic Simulations

The atmospheric cluster dynamic code (ACDC) (McGrath et al., 2012) was utilized to explore the cluster formation rates, growth pathways, and steady-state concentrations of the IA–MSA–DMA system by solving the birth-death equation (see the SI for details).

In the ACDC simulation, an enhancement factor of 2.3 was applied to the collision rate coefficient ( $\beta_{i,j}$ ) to account for enhanced intermolecular vdW forces (Halonen et al., 2019), consistent with its validated application in previous nucleation studies (Stolzenburg et al., 2020; Cai et al., 2021; Li et al., 2023; Ning et al., 2024). Additionally, the coagulation sink ( $S_i$ ) (Lehtipalo et al., 2016), which varies with cluster size, was calculated using Eq. (3):

$$S_i = CS_{ref} \times (d_i / d_{ref})^{-m}, \tag{3}$$

where  $CS_{ref}$  is the condensation sink (CS) of the reference monomer (*i.e.*, IA monomer), and d denotes the diameter of either the monomer or the cluster. The exponent m, set to 1.7, is dependent on the background aerosol distribution and falls within the typical range reported for atmospheric particles (Lehtinen et al., 2007). A cluster was defined as stable when the product of its collision rate coefficient and concentration ( $\beta$ ·C) surpasses the sum of its evaporation rate constants ( $\Sigma \gamma$ , Table S2). Such stable clusters were assumed to grow outside the simulated box without evaporating back into the system, and this criterion was applied to set the simulation boundary conditions (detailed in Table S3).

The condition settings for the ACDC simulations were based on data from field measurements, CLOUD experiments, and atmospheric modeling. For the marine boundary layer (MBL), the temperature (T) was primarily set within the range of 258 – 298 K (Almeida et al., 2013), and the CS was set as  $2.0 \times 10^{-3}$  s<sup>-1</sup> (He et al., 2021). The concentration range of precursors was specified as: [IA] =  $10^6 - 10^8$  molec. cm<sup>-3</sup> (Sipilä et al., 2016), [MSA] =  $10^6 - 10^8$  molec. cm<sup>-3</sup> (Chen et al., 2018; Berresheim et al., 2002; Ning et al., 2022a), and [DMA] = 0.025 - 2.5 pptv (Yu and Luo, 2014), respectively.

## 115 3 Results and Discussion

105

110

#### 3.1 Cluster Structure

Strong intermolecular noncovalent interactions are critical in governing the formation and stability of molecular clusters. To assess the synergistic nucleation potential of IA, MSA, and DMA, the surface electrostatic potential (ESP) mapped on van der Waals (vdW) surfaces of these molecules was analyzed using the Multiwfn 3.7 (Lu and Chen, 2012), based on the calculated



130

135



wavefunctions at the ωB97X-D/6-311++G(3df,3pd) (for C, H, O, N, and S atoms) + aug-cc-pVTZ-PP (for I atom) level of theory. The resulting ESP maps are presented in Fig. 1, where regions of positive and negative potential are depicted in red and blue, respectively. A positive ESP indicates an electrophilic region, suggesting a propensity to function as a donor in hydrogen bond (HB) or halogen bond (XB) interactions. In contrast, a negative ESP denotes a nucleophilic region, which is likely to serve as an acceptor in HB or XB interactions. A more detailed analysis is provided in the SI. ESP analysis demonstrates the potential for intermolecular interactions among IA, MSA, and DMA, thereby leading to further clustering.

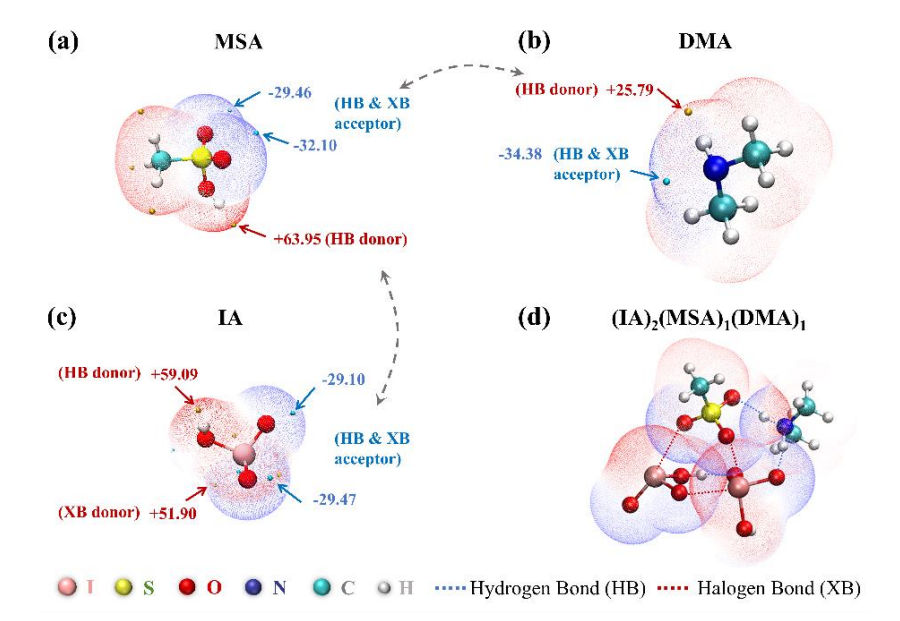


Figure 1. The ESP-mapped molecular vdW surface of (a) MSA, (b) DMA, (c) IA, and (d) (IA)<sub>2</sub>(MSA)<sub>1</sub>(DMA)<sub>1</sub> cluster at the ωB97X-D/6-311++G(3df,3pd) (for C, H, O, N, and S atoms) + aug-cc-pVTZ-PP (for I atom) level of theory. The golden and cyan dots represent the positions of maximums and minimums of ESP values (unit: kcal mol<sup>-1</sup>), respectively. The gray dashed arrows signify the site-to-site interaction tendencies.

To structurally elucidate the physicochemical nature of clustering, conformational analysis was performed to reveal the characters of intermolecular interactions within the identified ternary IA–MSA–DMA clusters (Fig. S1), where the red and black dashed lines denote XBs and HBs, respectively. The Cartesian coordinates of the optimized cluster structures are listed in Table S4. Overall, the resulting IA–MSA–DMA clusters are stabilized by a network of HBs and XBs. HBs are dominant, accounting for up to 74%, across all optimized ternary IA–MSA–DMA clusters. Two types of HBs (N–H···O and O–H···O) are observed, with N–H···O HBs dominating (71%) among the total HB interactions identified and typically forming between acids (IA and MSA) and base (DMA). Additionally, both MSA and DMA has methyl groups (–CH<sub>3</sub>) that are generally located on the periphery of clusters. This spatial arrangement facilitates the formation of HBs and XBs, reducing steric hindrance, promoting clustering, and enhancing stability.





During cluster formation, acid-base reactions between acid molecules (IA and MSA) and the base molecule (DMA) often occur, resulting in proton transfer and the formation of ion pairs such as IO<sub>3</sub><sup>-</sup>–DMAH<sup>+</sup> and CH<sub>3</sub>SO<sub>3</sub><sup>-</sup>–DMAH<sup>+</sup>. Given that MSA (pK<sub>a</sub> = -1.9) is a stronger acid than IA (pK<sub>a</sub> = 0.8), DMA preferentially undergoes protonation by MSA, forming the CH<sub>3</sub>SO<sub>3</sub><sup>-</sup>–DMAH<sup>+</sup> ion pair. This acid-base interaction not only strengthens the cluster via enhanced electrostatic stabilization but also introduces additional interaction sites for noncovalent bonding. As shown in Fig. S2, numerous unoccupied HB and XB sites are present in (IA)<sub>3</sub>(MSA)<sub>1</sub>(DMA)<sub>2</sub> cluster, which can further promote the condensation of atmospheric precursors and the growth of the cluster. These results indicate that IA, MSA, and DMA are capable of forming stable molecular clusters via HBs and XBs, accompanied by acid-base reactions that produce ion pairs.

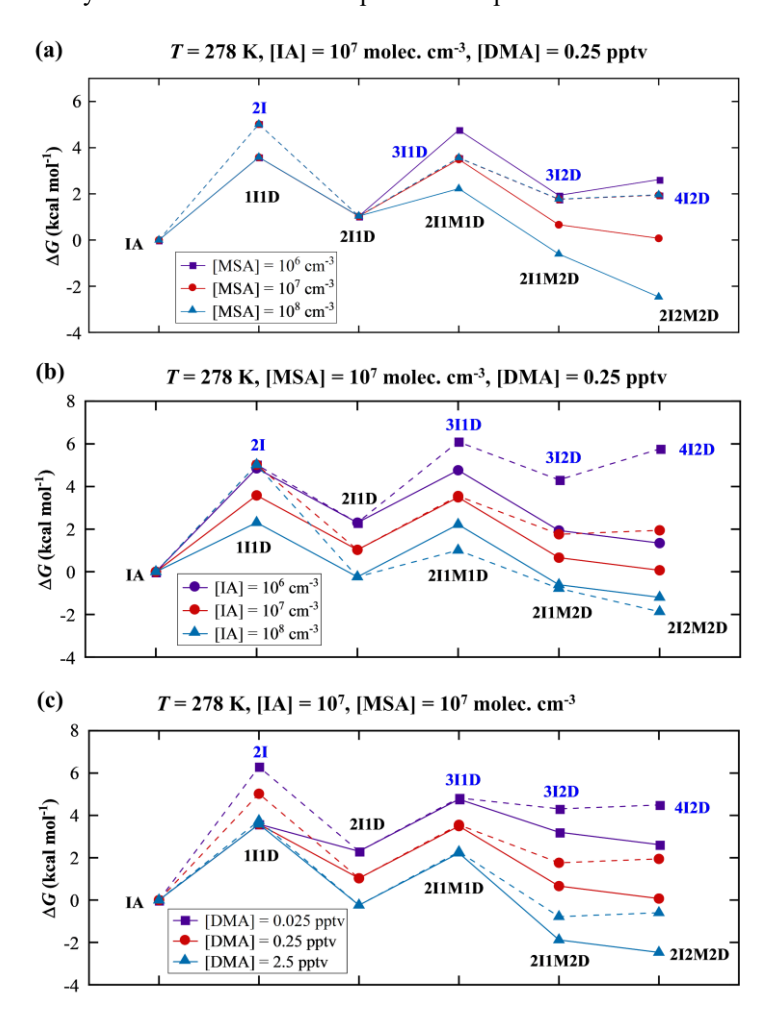


Figure 2. Gibbs free energies of cluster formation ( $\Delta G$ , kcal mol<sup>-1</sup>) based on the formation pathway of IA–MSA–DMA ternary (solid lines) 150 and IA–DMA binary (dashed lines) pathways at T = 278 K, (a) [MSA] =  $10^6 - 10^8$  molec. cm<sup>-3</sup>, (b) [IA] =  $10^6 - 10^8$  molec. cm<sup>-3</sup>, (c) [DMA] = 0.025 - 2.5 pptv. I: IA, M: MSA, D: DMA.



155

160

165

170

175

180



## 3.2 Cluster Stability

To evaluate the thermodynamic stability of the formed IA–MSA–DMA clusters, concentration-dependent Gibbs free energies  $(\Delta G, \text{Eq.}(2))$  were calculated, and free-energy profiles of the IA–MSA–DMA (ternary) and IA–DMA (binary) pathways were compared under varying precursor concentrations (Fig. 2). Overall, cluster formation energy barriers decrease with increasing precursor concentrations. The key distinction between the IA–MSA–DMA ternary and IA–DMA binary pathway arises in the step where the  $(IA)_2(DMA)_1$  cluster grows into either a  $(IA)_3(DMA)_1$  or a  $(IA)_2(MSA)_1(DMA)_1$  cluster. Thus, our discussion focuses on this critical step.

In Fig. 2(a) (T = 278 K), as [MSA] increases from  $10^6$  to  $10^8$  molec. cm<sup>-3</sup>, the barrier for the  $(IA)_2(DMA)_1 + IA \rightarrow (IA)_3(DMA)_1$  remains constant at 2.54 kcal mol<sup>-1</sup>, as this step is unaffected by MSA. In contrast,  $(IA)_2(DMA)_1 + MSA \rightarrow (IA)_2(MSA)_1(DMA)_1$  requires 3.73 kcal mol<sup>-1</sup> at [MSA] =  $10^6$  molec. cm<sup>-3</sup>, decreases to a level comparable to  $(IA)_3(DMA)_1$  formation at [MSA] =  $10^7$  molec. cm<sup>-3</sup> (but yields the more stable  $(IA)_2(MSA)_2(DMA)_2$  cluster), and further declines to 1.20 kcal mol<sup>-1</sup> at [MSA] =  $10^8$  molec. cm<sup>-3</sup>. These results clearly indicate that higher [MSA] facilitates the IA–MSA–DMA ternary pathway. As shown in Fig. 2(b), at  $[IA] = 10^6$  molec. cm<sup>-3</sup>, formation of  $(IA)_2(MSA)_1(DMA)_1$  cluster (2.47 kcal mol<sup>-1</sup>) is energetically more favorable than  $(IA)_3(DMA)_1$  cluster (3.80 kcal mol<sup>-1</sup>), whereas at  $[IA] = 10^8$  molec. cm<sup>-3</sup>, the opposite occurs. This suggests that, unlike [MSA], lower [IA] favors the IA–MSA–DMA pathway. In Fig. 2(c), the energy barriers of the IA–MSA–DMA and IA–DMA pathways are identical at the same [DMA], as the transformation from  $(IA)_2(DMA)_1$  cluster to either  $(IA)_3(DMA)_1$  or  $(IA)_2(MSA)_1(DMA)_1$  cluster proceeds without the involvement of an additional DMA monomer. However, the resulting  $(IA)_2(MSA)_2(DMA)_2$  cluster is more stable than  $(IA)_4(DMA)_2$ , indicating that as [DMA] increases from 0.025 to 2.5 pptv, the IA–MSA–DMA pathway predominates. These results indicate that the IA–MSA–DMA pathway is thermodynamically more favorable under the conditions with abundant MSA and DMA but limited IA.

## 3.3 Cluster Formation Rate

To assess the potential synergistic enhancement, the cluster formation rate  $(J, \text{cm}^{-3} \text{ s}^{-1})$  of the IA–MSA–DMA system was calculated and compared with the previously reported efficient IA–DMA system (Ning et al., 2022b) using ACDC simulations. As illustrated in Fig. 3(a), the simulated J of IA–DMA and IA–MSA–DMA systems exhibit a positive correlation with increasing [IA] under the marine boundary layer (MBL) conditions of T = 278 K, CS =  $2.0 \times 10^{-3}$  s<sup>-1</sup>, [MSA] =  $10^6 - 10^8$  molec. cm<sup>-3</sup>, and [DMA] = 0.25 pptv. In comparison, the IA–MSA–DMA system exhibits significantly higher J values than the IA–DMA system, with similar J observed only at high [IA] (>  $10^7$  molec. cm<sup>-3</sup>) and low [MSA] ( $10^6$  molec. cm<sup>-3</sup>), showing a pronounced synergistic enhancement in nucleation. As long as [IA] drops below  $10^7$  molec. cm<sup>-3</sup>, IA–MSA–DMA system shows markedly faster nucleation than IA–DMA system, even at the low level of [MSA] ( $10^6$  molec. cm<sup>-3</sup>). At a moderate [MSA] ( $10^7$  molec. cm<sup>-3</sup>), the J(IA–MSA–DMA) reaches the order of  $10^0 - 10^2$  cm<sup>-3</sup> s<sup>-1</sup>, which is up to  $10^3$  times higher than J(IA–DMA) under the same conditions. Apart from the synergistic effects exhibited by IA–MSA–DMA ternary nucleation, we further compared the nucleation efficiencies of the binary acid–base system: IA–DMA and MSA–DMA systems.



185

190

195

200



Interestingly, although IA exhibits weaker acidity compared to MSA, the resulting J of IA–DMA system significantly exceeds that of the MSA–DMA system by up to approximately four orders of magnitude at same acid levels (Fig. S3). The difference arises from the generally lower  $\Delta G$ s of IA–DMA clusters relative to MSA–DMA clusters with the same number of molecules, possibly due to the presence of not only HBs but also XBs, which provide additional structural stabilization. Taken together, these findings highlight the enhanced nucleation efficiency arising from the synergistic interactions among MSA, IA, and DMA.

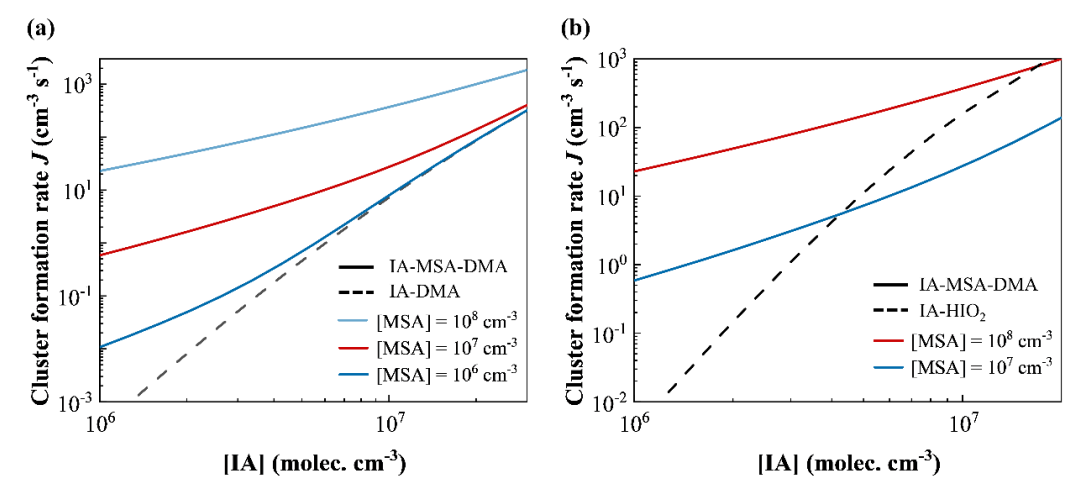


Figure 3. (a) Cluster formation rates J (cm<sup>-3</sup> s<sup>-1</sup>) of the IA–DMA and IA–MSA–DMA systems under conditions of T = 278 K, CS =  $2.0 \times 10^{-3}$  s<sup>-1</sup>, [IA] =  $10^6 - 3.0 \times 10^7$  molec. cm<sup>-3</sup>, [MSA] =  $10^6 - 10^8$  molec. cm<sup>-3</sup>, and [DMA] = 0.25 pptv; (b) J of the IA–HIO<sub>2</sub> and IA–MSA–DMA systems under conditions of T = 278 K, CS =  $2.0 \times 10^{-3}$  s<sup>-1</sup>, [IA] =  $10^6 - 2.0 \times 10^7$  molec. cm<sup>-3</sup>, [MSA] =  $10^7 - 10^8$  molec. cm<sup>-3</sup>, and [DMA] = 0.25 pptv. [IA]/[HIO<sub>2</sub>] is fixed at a value of 50.

To clarify atmospheric relevance of IA–MSA–DMA nucleation in the MBL, the simulated J(IA-MSA-DMA) was compared with that of the well-established IA-iodous acid (HIO<sub>2</sub>) system, which has been proposed as a key nucleation mechanism in the MBL (He et al., 2021; Liu et al., 2023; Zhang et al., 2022). As shown in Fig. 3(b), at [MSA] =  $10^7$  molec. cm<sup>-3</sup>, the IA–MSA–DMA system exhibits notably higher J values than the IA–HIO<sub>2</sub> system at lower [IA] (<  $4 \times 10^6$  molec. cm<sup>-3</sup>), although the latter slightly surpasses the former under higher [IA] conditions. However, when [MSA] increases to  $10^8$  molec. cm<sup>-3</sup>, the values of J(IA-MSA-DMA) are almost higher than the  $J(IA-HIO_2)$  at the range of [IA] ( $10^6-10^7$  molec. cm<sup>-3</sup>), with rate enhancements reaching up to four orders of magnitude. This indicates that the proposed IA–MSA–DMA system also represents a highly efficient nucleation mechanism in the MBL. Collectively, these results highlight the critical role of the synergistic nucleation involving MSA, IA, and DMA, suggesting that IA–MSA–DMA nucleation could represent a key mechanism in MBL. This mechanism serves as a critical yet overlooked source of fresh particles in the MBL.





## 205 3.4 Synergistic Nucleation of IA, MSA, and DMA

As discussed above, the IA-MSA-DMA system shows a synergistic effect on nucleation, resulting in an enhancement on J. To access this, the included most efficient binary system, i.e., IA-DMA nucleation, was selected as a reference for comparison. Herein, we accordingly define the enhancement factor R as the ratio of J(IA-MSA-DMA) to J(IA-DMA) (Eq. (4)).

$$R = \frac{J(\text{IA} - \text{MSA} - \text{DMA})}{J(\text{IA} - \text{DMA})} = \frac{J([\text{IA}] = x, [\text{MSA}] = y, [\text{DMA}] = z)}{J([\text{IA}] = x, [\text{MSA}] = 0, [\text{DMA}] = z)},$$
(4)

210 where x, y, and z denote the concentrations of IA, MSA, and DMA, respectively.

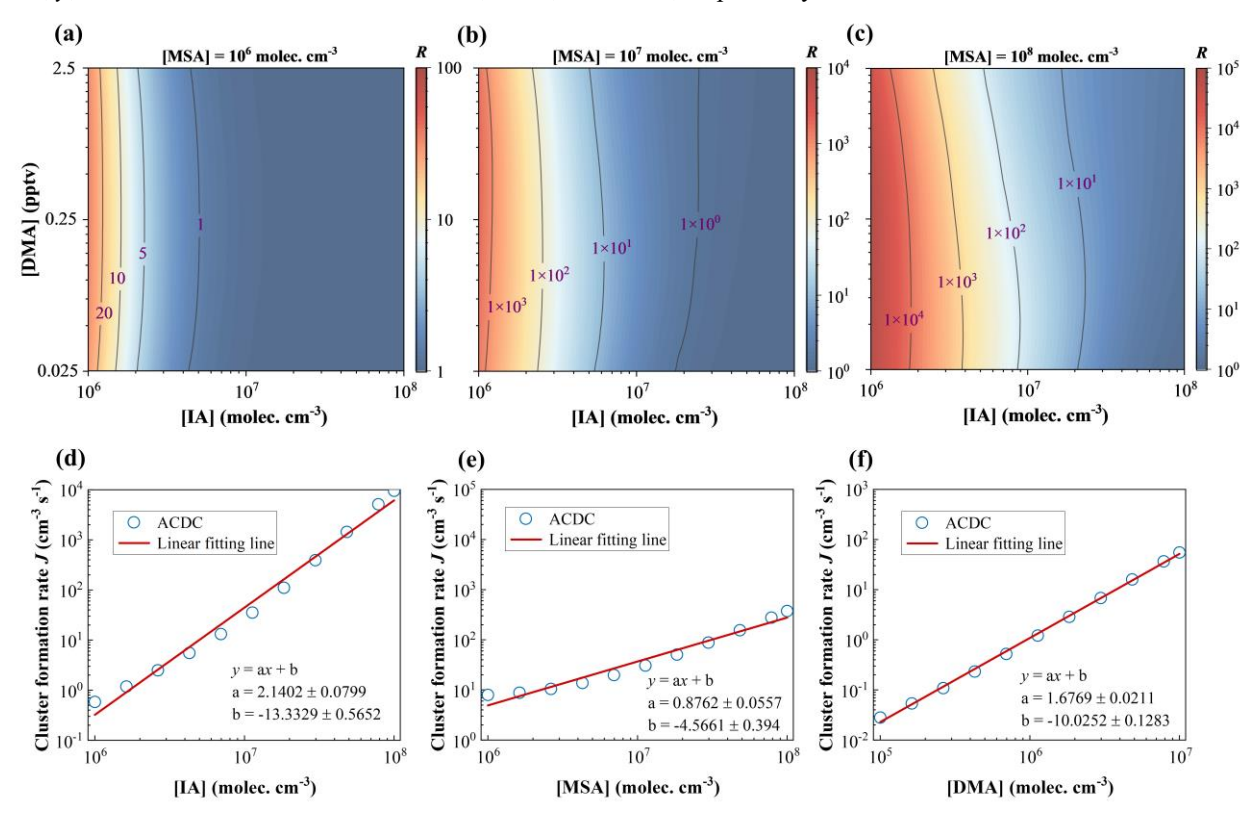


Figure 4. Enhancement factor R for IA-MSA-DMA cluster formation under conditions of T = 278 K, CS =  $2.0 \times 10^{-3}$  s<sup>-1</sup>, [IA] =  $10^6 - 10^8$  molec. cm<sup>-3</sup>, [DMA] = 0.025 - 2.5 pptv, and (a) [MSA] =  $10^6$ , (b)  $10^7$ , and (c)  $10^8$  molec. cm<sup>-3</sup>, respectively. Function dependence of the cluster formation rate (J) on (d) [IA], (e) [MSA], and (f) [DMA], showing a linear relationship.

As shown in Fig. 4(a)-(c), the calculated *R* increases with rising MSA levels (10<sup>6</sup> to 10<sup>8</sup> molec. cm<sup>-3</sup>), spanning 1 to 4 orders of magnitude, highlight the efficiency of ternary nucleation. In contrast, with [MSA] and [DMA] held constant, *R* decreases markedly as [IA] increases. This trend aligns with Fig. 3(a), the gap between *J*(IA–MSA–DMA) to *J*(IA–DMA) narrows with rising [IA]. It may be explained by IA's higher efficiency in binding DMA compared to MSA (recalling Sect. 3.3 and Fig. S3), coupled with higher [IA], which amplifies the role of IA–DMA nucleation. While *R* is less sensitive to [DMA]



240

245

250



compared to [IA], likely due to the relatively narrow range of [DMA] in atmosphere, which constrains its impact. Overall, the *R* gradually decreases with increasing [IA]. However, at higher [MSA], a slight increase in *R* is observed, as the presence of MSA counteracts the dominance of the strong IA–DMA binding and enhances the stability of the ternary clusters. And the IA–MSA–DMA synergistic nucleation rate shows a sensitivity ranking of IA > DMA > MSA with respect to their concentration variations (Fig. 4(d)-(f)). These findings suggest that IA–MSA–DMA synergistic nucleation is most effective in iodine-limited, sulfur-, and nitrogen-rich regions.

### 3.5 Cluster Formation Pathway

As indicated by the rate analyses, the IA-MSA-DMA synergy enhances nucleation; however, the underlying clustering pathways and their corresponding contribution to particle formation remain unresolved, necessitating further analysis to clarify nucleation dynamics.

As illustrated in Fig. 5(a), under the potential MBL conditions of T = 278 K,  $CS = 2.0 \times 10^{-3}$  s<sup>-1</sup>, [IA] =  $10^7$  molec. cm<sup>-3</sup>, [MSA] =  $10^7$  molec. cm<sup>-3</sup>, and [DMA] = 0.25 pptv, the cluster formation pathways of IA–MSA–DMA system can be classified into two types: IA–DMA binary pathway and IA–MSA–DMA ternary pathway. Specifically, IA–DMA clustering pathway proceeds primarily by sequential collisions of IA and DMA monomers, ultimately forming (IA)<sub>4</sub>(DMA)<sub>2</sub> cluster that is recognized as the boundary cluster (see details in the SI), which can grow beyond the simulation system. This part of pathways are similar to that revealed by Ning et al. (2022b).

In contrast, the ternary IA-MSA-DMA clustering pathway is more complex. In addition to a stepwise growth route similar to the binary IA-DMA pathway via  $(IA)_2(DMA)_1$  cluster, IA monomer can also collide with MSA monomer to form a  $(IA)_1(MSA)_1$  heterodimer. The formed  $(IA)_1(MSA)_1$  cluster can further collide with DMA monomer to form a  $(IA)_1(MSA)_1(DMA)_1$  heterotrimer, which can grow via two routes: a) colliding with an IA monomer to produce a  $(IA)_2(MSA)_1(DMA)_1$  cluster; b) colliding with a MSA monomer to form a  $(IA)_1(MSA)_2(DMA)_1$  cluster. The two clusters can continue to grow, ultimately yielding a  $(IA)_2(MSA)_2(DMA)_2$  cluster, which can grow larger to contribute to particle formation. At elevated temperatures of 288 - 298 K, the IA-MSA-DMA ternary nucleation pathway exhibits notable modifications. As illustrated in Fig. S4, both IA and MSA monomers are capable of alternately colliding with other monomers, ultimately yielding the  $(IA)_1(MSA)_2(DMA)_3$  cluster that subsequently undergoes further growth.

To further quantify the relative contributions of different clustering pathways, we performed ACDC simulations to track the molecular-level clustering processes under varying precursor concentrations and temperatures. As shown in Fig. 5(b), the contribution of the IA–MSA–DMA pathway (yellow bar) exhibits a pronounced positive dependence on both [MSA] and [DMA]. Specifically, as [MSA] increases from  $5.0 \times 10^5$  to  $5.0 \times 10^7$  molec. cm<sup>-3</sup>, the contribution of IA–MSA–DMA pathway rises sharply from 3% to 98%. Similarly, increasing [DMA] from  $2.5 \times 10^{-3}$  to  $2.5 \times 10^{-2}$  pptv results in a substantial enhancement of the pathway contribution from 20% to 67%; however, further elevation of [DMA] to  $2.5 \times 10^{-1}$  and  $2.5 \times 10^{0}$  pptv induces only marginal changes, suggesting a base saturation effect. In contrast, the contribution of the IA–MSA–DMA pathway is negatively correlated with [IA]. At [IA] below  $10^7$  molec. cm<sup>-3</sup>, the ternary IA–MSA–DMA pathway predominates,



255



whereas at [IA] above this threshold, the binary IA–DMA pathway becomes dominant. Temperature also exerts a significant influence: as the temperature increases from 258 K to 298 K, the relative contribution of the IA–MSA–DMA pathway decreases markedly, with an abrupt decline observed between 278 K and 288 K. This may be attributed to a distinct change in the growth pattern of the IA–MSA–DMA pathway when the temperature rises to 288 – 298 K (Fig. S5).

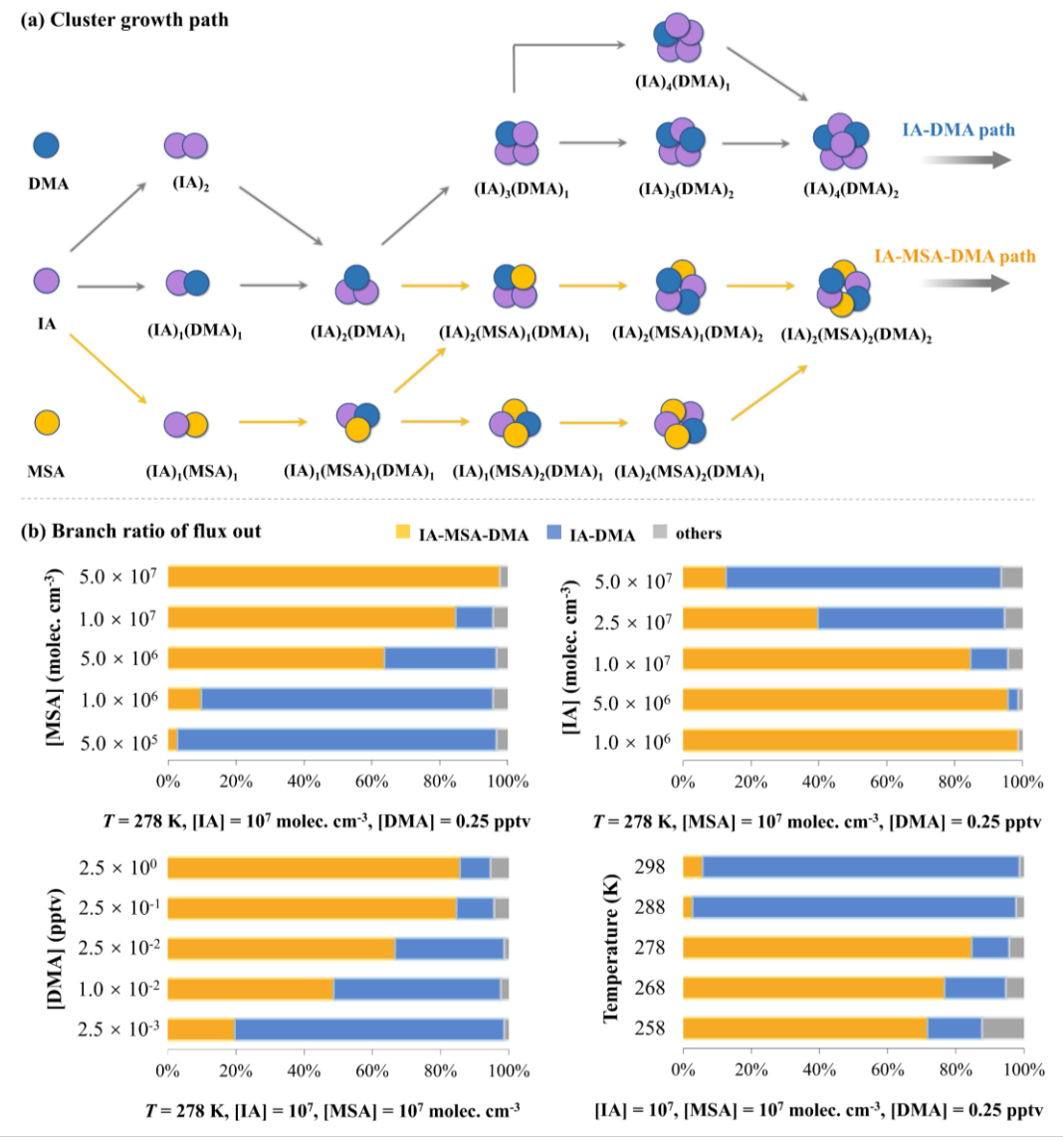


Figure 5. (a) The simulated primary cluster growth pathways of IA–MSA–DMA system at the conditions of T = 278 K, CS =  $2.0 \times 10^{-3}$  s<sup>-1</sup>, [IA] =  $10^7$  molec. cm<sup>-3</sup>, [MSA] =  $10^7$  molec. cm<sup>-3</sup>, and [DMA] = 0.25 ppty; (b) Branch ratio of different flux out under the varying [MSA] ( $5.0 \times 10^5 - 5.0 \times 10^7$  molec. cm<sup>-3</sup>), [IA] ( $1.0 \times 10^6 - 5.0 \times 10^7$  molec. cm<sup>-3</sup>), [DMA] ( $2.5 \times 10^{-3} - 2.5 \times 10^0$  pptv), and temperatures (258 - 298 K).



265

275



Overall, these results demonstrate that the IA-MSA-DMA pathway is highly sensitive to precursor concentrations and temperatures. Its contribution increases strongly with [MSA] and moderately with [DMA] until a saturation effect is reached, while exhibiting a negative dependence on [IA]. Temperature rise significantly suppresses the role of this ternary pathway, especially around 278 – 288 K. Therefore, this synergistic nucleation of sulfur (MSA), iodine (IA), and nitrogen (DMA) precursors is most prevalent in cold environments that are rich in sulfur and nitrogen but scarce in iodine, such as polar marine regions, as previous studies have shown that the MSA formation is highly temperature-dependent, being more favorable in polar areas (Chen et al., 2023) and IA concentrations decreases significantly at high latitudes with lower temperatures (He et al., 2021).

## 270 3.6 Comparison with Field Observations

To better evaluate the potential atmospheric implications of the proposed IA–MSA–DMA nucleation mechanism, we calculated the cluster formation rate under polar conditions, where the impact of IA–MSA–DMA nucleation is expected to be significant, and further compared the simulations with field observations. As discussed earlier, the IA–MSA–DMA synergistic nucleation is relatively impactful in the cold coastal regions, where [MSA] is relatively higher and [IA] is lower. Accordingly, Marambio and Aboa were selected for a comparative analysis due to their shared characteristics: both sites are located in coastal polar regions, exhibit high [MSA] levels but relatively low [IA], and have low annual mean temperatures ( $\leq 273$  K) (Quéléver et al., 2022; Xavier et al., 2024).

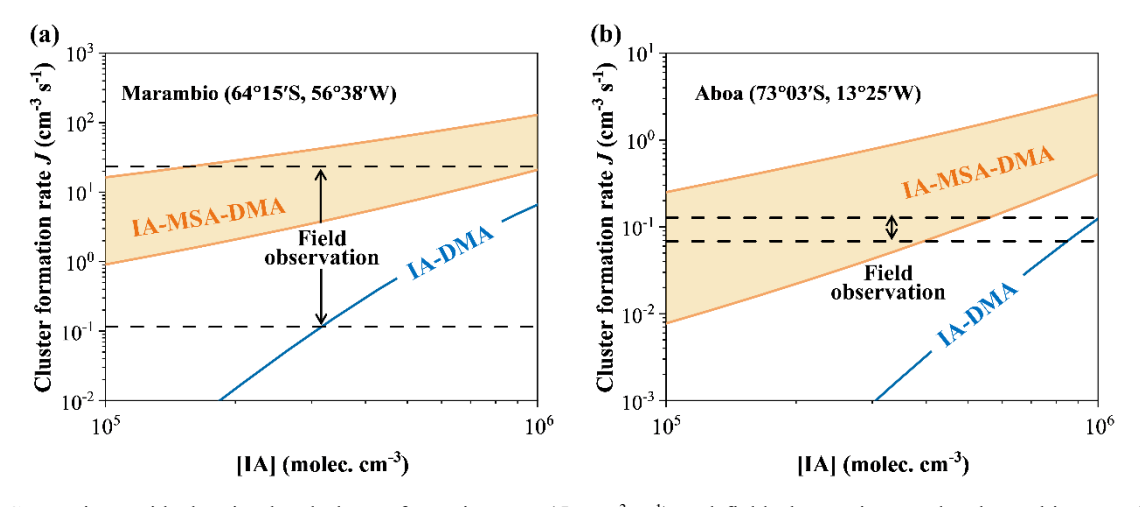


Figure 6. Comparison with the simulated cluster formation rate  $(J, \text{ cm}^{-3} \text{ s}^{-1})$  and field observations under the ambient conditions: (a) Marambio  $(T = 273 \text{ K}, \text{CS} = 10^{-4} \text{ s}^{-1}, [\text{IA}] = 10^5 - 10^6 \text{ molec. cm}^{-3}, [\text{MSA}] = 10^6 - 10^7 \text{ molec. cm}^{-3}, \text{ and } [\text{DMA}] = 2.0 \text{ pptv})$  and (b) Aboa  $(T = 268 \text{ K}, \text{CS} = 10^{-4} \text{ s}^{-1}, [\text{IA}] = 10^5 - 10^6 \text{ molec. cm}^{-3}, [\text{MSA}] = 10^6 - 10^7 \text{ molec. cm}^{-3}, \text{ and } [\text{DMA}] = 0.055 \text{ pptv})$ . The orange area, blue line, and black line represent J(IA-MSA-DMA), J(IA-DMA), and J(field observation), respectively.

As illustrated in Fig. 6(a), the J(IA-MSA-DMA) was simulated under the representative atmospheric conditions of T = 273 K,  $CS = 10^{-4} \text{ s}^{-1}$ ,  $[IA] = 10^5 - 10^6 \text{ molec. cm}^{-3}$ ,  $[MSA] = 10^6 - 10^7 \text{ molec. cm}^{-3}$ , and [DMA] = 2.0 pptv (Quéléver et al.,





2022; He et al., 2021; Yu and Luo, 2014). The simulated values of *J* were then compared with field-measured nucleation rates at the coastal Antarctic station Marambio. The results show that, for both the IA–DMA and IA–MSA–DMA systems, the *J* increases monotonically with [IA]. Notably, the incorporation of MSA markedly enhances the formation rates (orange-shaded region), bringing them into closer alignment with the observed nucleation rate range (0.12 – 24 cm<sup>-3</sup> s<sup>-1</sup>, black dashed lines) (Quéléver et al., 2022). Even at the lower bound of [MSA] (10<sup>6</sup> molec. cm<sup>-3</sup>, lower orange solid line), the simulated formation rate exceeds the minimum observed value (0.12 cm<sup>-3</sup> s<sup>-1</sup>, lower black dashed line) by more than one order of magnitude.

A further comparison was conducted under conditions representative of the Aboa station, at T = 268 K,  $CS = 10^{-4}$  s<sup>-1</sup>,  $[IA] = 10^5 - 10^6$  molec. cm<sup>-3</sup>,  $[MSA] = 10^6 - 10^7$  molec. cm<sup>-3</sup>, and [DMA] = 0.055 pptv (Xavier et al., 2024; He et al., 2021; Yu and Luo, 2014), with the corresponding results shown in Fig. 6(b). The simulated J values of the IA–MSA–DMA system partially overlap with the field observation rates  $(0.07 - 0.13 \text{ cm}^{-3} \text{ s}^{-1})$ , black dashed lines) (Xavier et al., 2024), whereas the simulated J(IA-DMA) values deviate considerably from the observations. These results underscore the potential importance of the synergistic nucleation of sulfur-, iodine-, and nitrogen-containing compounds in cold polar marine environments, particularly during periods of elevated sulfur compound concentrations associated with NPF events.

#### 4 Conclusion

295

300

305

310

315

Marine aerosol significantly influences the Earth's radiative balance and climate system, yet the fundamental nucleation mechanism in aerosol formation is highly unclear. Despite the recognition of sulfur-, iodine-, and nitrogen-containing chemicals as vital nucleating precursors, whether they can interact and synergistically contribute to nucleation remains unknown.

To address this gap, we systematically investigated the ternary nucleation system involving methanesulfonic acid (MSA, sulfur-containing), iodic acid (IA, iodine-containing), and dimethylamine (DMA, nitrogen-containing) via high-level quantum chemical calculations and atmospheric cluster dynamics simulations. The main findings of this study are as follows: (1) the stable prenucleation cluster composed of IA, MSA, and DMA is mainly stabilized by intermolecular hydrogen bonds (74%), together with contributions from halogen bonding (XB) and electrostatic attractions between ion pairs produced via acid—base reactions (i.e., CH<sub>3</sub>SO<sub>3</sub><sup>-</sup>–DMAH<sup>+</sup> and IO<sub>3</sub><sup>-</sup>–DMAH<sup>+</sup>). (2) The nucleation dynamics of the IA-MSA-DMA system exhibits a pronounced synergistic effect, leading to an enhancement in nucleation rates by 4–8 orders of magnitude compared with the included binary IA–DMA or MSA–DMA systems; under sulfur-rich conditions, the resulting rate even surpasses that of the efficient IA–iodous acid (HIO<sub>2</sub>) nucleation mechanism. (3) Mechanistic analysis indicates that the IA-MSA-DMA ternary nucleation is most evident under cold, sulfur- and nitrogen-rich conditions, and the simulated rates under polar-site conditions (Marambio and Aboa) align well with field observations, advancing our understanding of NPF events.

These results advance our understanding of marine nucleation by highlighting the synergistic role of sulfur, iodine, and nitrogen precursors—an effect that was previously ignored in binary nucleation frameworks. Incorporating the IA-MSA-

https://doi.org/10.5194/egusphere-2025-5622 Preprint. Discussion started: 20 November 2025

© Author(s) 2025. CC BY 4.0 License.





DMA mechanism into atmospheric models can refine parameterizations of marine aerosol formation, reducing uncertainties in climate forcing predictions.

**Data availability.** The data in this article are available from the corresponding author upon reasonable request (anning@bit.edu.cn and zhangxiuhui@bit.edu.cn).

320 **Supplement.** The supplement related to this article is available online at:

**Author contribution.** XZ designed and supervised the research. JL, XD, and AN performed the quantum chemical calculations and the ACDC simulations. JL, AN, and LL analyzed data. JL, AN, and XZ wrote the paper with contributions from all the other co-authors.

Competing interests. The contact author has declared that neither they nor their co-authors have any competing interests.

325 **Disclaimer.** Publisher's note: Copernicus Publications remains neutral with regard to jurisdictional claims in published maps and institutional affiliations.

**Acknowledgement.** This work is funded by the National Science Fund for Distinguished Young Scholars (grant no. 22225607), the National Natural Science Foundation of China (grant nos. 22306011 and 22376013).

**Financial support.** This work is supported by the National Science Fund for Distinguished Young Scholars (grant no. 22225607) and the National Natural Science Foundation of China (grant nos. 22306011 and 22376013).

# References

335

Almeida, J., Schobesberger, S., Kürten, A., Ortega, I. K., Kupiainen-Määttä, O., Praplan, A. P., Adamov, A., Amorim, A., Bianchi, F., Breitenlechner, M., David, A., Dommen, J., Donahue, N. M., Downard, A., Dunne, E., Duplissy, J., Ehrhart, S., Flagan, R. C., Franchin, A., Guida, R., Hakala, J., Hansel, A., Heinritzi, M., Henschel, H., Jokinen, T., Junninen, H., Kajos, M., Kangasluoma, J., Keskinen, H., Kupc, A., Kurten, T., Kvashin, A. N., Laaksonen, A., Lehtipalo, K., Leiminger, M., Leppä, J., Loukonen, V., Makhmutov, V., Mathot, S., McGrath, M. J., Nieminen, T., Olenius, T., Onnela, A., Petäjä, T., Riccobono, F., Riipinen, I., Rissanen, M., Rondo, L., Ruuskanen, T., Santos, F. D., Sarnela, N., Schallhart, S., Schnitzhofer, R., Seinfeld, J. H., Simon, M., Sipilä, M., Stozhkov, Y., Stratmann, F., Tomé, A., Tröstl, J., Tsagkogeorgas,



345



- G., Vaattovaara, P., Viisanen, Y., Virtanen, A., Vrtala, A., Wagner, P. E., Weingartner, E., Wex, H., Williamson, C., Wimmer, D., Ye, P., Yli-Juuti, T., Carslaw, K. S., Kulmala, M., Curtius, J., Baltensperger, U., Worsnop, D. R., Vehkamäki, H. and Kirkby, J.: Molecular understanding of sulphuric acid-amine particle nucleation in the atmosphere, Nature, 502, 359–363, http://doi.org/10.1038/nature12663, 2013.
  - Baccarini, A., Karlsson, L., Dommen, J., Duplessis, P., Vullers, J., Brooks, I. M., Saiz-Lopez, A., Salter, M., Tjernstrom, M., Baltensperger, U., Zieger, P. and Schmale, J.: Frequent new particle formation over the high Arctic pack ice by enhanced iodine emissions, Nat. Commun., 11, 4924, http://doi.org/10.1038/s41467-020-18551-0, 2020.
  - Beck, L. J., Sarnela, N., Junninen, H., Hoppe, C. J. M., Garmash, O., Bianchi, F., Riva, M., Rose, C., Peräkylä, O., Wimmer, D., Kausiala, O., Jokinen, T., Ahonen, L., Mikkilä, J., Hakala, J., He, X. C., Kontkanen, J., Wolf, K. K. E., Cappelletti, D., Mazzola, M., Traversi, R., Petroselli, C., Viola, A. P., Vitale, V., Lange, R., Massling, A., Nøjgaard, J. K., Krejci, R., Karlsson, L., Zieger, P., Jang, S., Lee, K., Vakkari, V., Lampilahti, J., Thakur, R. C., Leino, K., Kangasluoma, J., Duplissy,
- E. M., Siivola, E., Marbouti, M., Tham, Y. J., Saiz-Lopez, A., Petäjä, T., Ehn, M., Worsnop, D. R., Skov, H., Kulmala, M., Kerminen, V. M. and Sipilä, M.: Differing Mechanisms of New Particle Formation at Two Arctic Sites, Geophys. Res. Lett., 48, e2020GL091334, http://doi.org/10.1029/2020gl091334, 2021.
  - Berresheim, H., Elste, T., Rosman, K., Dal Maso, M., Tremmel, H. G., Mäkelä, J. M., Allen, A. G., Kulmala, M. and Hansson, H.-C.: Gas-aerosol relationships of H<sub>2</sub>SO<sub>4</sub>, MSA, and OH: Observations in the coastal marine boundary layer at Mace Head, Ireland, J. Geophys. Res.-Atmos., 107, PAR 5-1–PAR 5-12, http://doi.org/10.1029/2000jd000229, 2002.
  - Cai, R., Yan, C., Yang, D., Yin, R., Lu, Y., Deng, C., Fu, Y., Ruan, J., Li, X., Kontkanen, J., Zhang, Q., Kangasluoma, J., Ma, Y., Hao, J., Worsnop, D. R., Bianchi, F., Paasonen, P., Kerminen, V.-M., Liu, Y., Wang, L., Zheng, J., Kulmala, M. and Jiang, J.: Sulfuric acid–amine nucleation in urban Beijing, Atmos. Chem. Phys., 21, 2457–2468, http://doi.org/10.5194/acp-21-2457-2021, 2021.
- Chan, B. and Yim, W. L.: Accurate Computation of Cohesive Energies for Small to Medium-Sized Gold Clusters, J. Chem. Theory Comput., 9, 1964–1970, http://doi.org/10.1021/ct400047y, 2013.
  - Chen, H. and Finlayson-Pitts, B. J.: New Particle Formation from Methanesulfonic Acid and Amines/Ammonia as a Function of Temperature, Environ Sci Technol, 51, 243-252, http://doi.org/10.1021/acs.est.6b04173, 2017.
- Chen, H., Varner, M. E., Gerber, R. B. and Finlayson-Pitts, B. J.: Reactions of Methanesulfonic Acid with Amines and Ammonia as a Source of New Particles in Air, J. Phys. Chem. B, 120, 1526–1536, http://doi.org/10.1021/acs.jpcb.5b07433, 2016.
  - Chen, J., Lane, J. R., Bates, K. H. and Kjaergaard, H. G.: Atmospheric Gas-Phase Formation of Methanesulfonic Acid, Environ. Sci. Technol., 57, 21168–21177, http://doi.org/10.1021/acs.est.3c07120, 2023.
- Chen, Q., Sherwen, T., Evans, M. and Alexander, B.: DMS oxidation and sulfur aerosol formation in the marine troposphere: a focus on reactive halogen and multiphase chemistry, Atmos. Chem. Phys., 18, 13617–13637, http://doi.org/10.5194/acp-18-13617-2018, 2018.





- Dal Maso, M., Kulmala, M., Lehtinen, K. E. J., Mäkelä, J. M., Aalto, P. and O'Dowd, C. D.: Condensation and coagulation sinks and formation of nucleation mode particles in coastal and boreal forest boundary layers, J. Geophys. Res.-Atmos., 107, PAR 2-1–PAR 2-10, http://doi.org/10.1029/2001jd001053, 2002.
- Dawson, M. L., Varner, M. E., Perraud, V., Ezell, M. J., Gerber, R. B. and Finlayson-Pitts, B. J.: Simplified mechanism for new particle formation from methanesulfonic acid, amines, and water via experiments and ab initio calculations, Proc. Natl. Acad. Sci. U. S. A., 109, 18719–18724, http://doi.org/10.1073/pnas.1211878109, 2012.
  - Eisele, F. L. and Tanner, D. J.: Measurement of the gas phase concentration of H<sub>2</sub>SO<sub>4</sub> and methane sulfonic acid and estimates of H<sub>2</sub>SO<sub>4</sub> production and loss in the atmosphere, J. Geophys. Res., 98, 9001–9010, http://doi.org/10.1029/93JD00031, 1993.
- 380 Elm, J.: Clusteromics II: Methanesulfonic acid-base cluster formation, ACS Omega, 6, 17035–17044, http://doi.org/10.1021/acsomega.1c02115, 2021.
  - Engsvang, M. and Elm, J.: Iodine Clusters in the Atmosphere II: Cluster Formation Potential of Iodine Oxyacids and Iodine Oxides, ACS Omega, 10, 24887-24896, http://doi.org/10.1021/acsomega.5c02147, 2025.
  - Engsvang, M., Wu, H. and Elm, J.: Iodine clusters in the atmosphere I: Computational benchmark and dimer formation of oxyacids and oxides, ACS Omega, 9, 31521–31532, http://doi.org/10.1021/acsomega.4c01235, 2024.
    - Francl, M. M., Pietro, W. J., Hehre, W. J., Binkley, J. S., Gordon, M. S., DeFrees, D. J. and Pople, J. A.: Self-consistent molecular orbital methods. XXIII. A polarization-type basis set for second-row elements, J. Chem. Phys., 77, 3654–3665, http://doi.org/10.1063/1.444267, 1982.
- Frisch, M. J., Trucks, G. W., Schlegel, H. B., Scuseria, G. E., Robb, M. A., Cheeseman, J. R., Scalmani, G., Barone, V.,
  Mennucci, B., Petersson, G. A., Nakatsuji, H., Caricato, M., Li, X., Hratchian, H. P., Izmaylov, A. F., Bloino, J., Zheng,
  G., Sonnenberg, J. L., Hada, M., Ehara, M., Toyota, K., Fukuda, R., Hasegawa, J., Ishida, M., Nakajima, T., Honda, Y.,
  Kitao, O., Nakai, H., Vreven, T., Montgomery, J. A., Peralta, J. E., Ogliaro, F., Bearpark, M., Heyd, J. J., Brothers, E.,
  Kudin, K. N., Staroverov, V. N., Kobayashi, R., Normand, J., Raghavachari, K., Rendell, A., Burant, J. C., Iyengar, S. S.,
  Tomasi, J., Cossi, M., Rega, N., Millam, J. M., Klene, M., Knox, J. E., Cross, J. B., Bakken, V., Adamo, C., Jaramillo, J.,
- Gomperts, R., Stratmann, R. E., Yazyev, O., Austin, A. J., Cammi, R., Pomelli, C., Ochterski, J. W., Martin, R. L., Morokuma, K., Zakrzewski, V. G., Voth, G. A., Salvador, P., Dannenberg, J. J., Dapprich, S., Daniels, A. D., Farkas, O., Foresman, J. B., Ortiz, J. V., Cioslowski, J. and Fox, D. J.: Gaussian 09, Revision A.02, Gaussian Inc, Wallingford CT, http://doi.org/gaussian.com/g09citation/ (last access: 7 May 2022), 2009.
- Frisch, M. J., Trucks, G. W., Schlegel, H. B., Scuseria, G. E., Robb, M. A., Cheeseman, J. R., Scalmani, G., Barone, V.,
  Mennucci, B., Petersson, G. A., Nakatsuji, H., Caricato, M., Li, X., Hratchian, H. P., Izmaylov, A. F., Bloino, J., Zheng,
  G., Sonnenberg, J. L., Hada, M., Ehara, M., Toyota, K., Fukuda, R., Hasegawa, J., Ishida, M., Nakajima, T., Honda, Y.,
  Kitao, O., Nakai, H., Vreven, T., Montgomery, J. A., Peralta, J. E., Ogliaro, F., Bearpark, M., Heyd, J. J., Brothers, E.,
  Kudin, K. N., Staroverov, V. N., Kobayashi, R., Normand, J., Raghavachari, K., Rendell, A., Burant, J. C., Iyengar, S. S.,
  Tomasi, J., Cossi, M., Rega, N., Millam, J. M., Klene, M., Knox, J. E., Cross, J. B., Bakken, V., Adamo, C., Jaramillo, J.,
- 405 Gomperts, R., Stratmann, R. E., Yazyev, O., Austin, A. J., Cammi, R., Pomelli, C., Ochterski, J. W., Martin, R. L.,





- Morokuma, K., Zakrzewski, V. G., Voth, G. A., Salvador, P., Dannenberg, J. J., Dapprich, S., Daniels, A. D., Farkas, O., Foresman, J. B., Ortiz, J. V., Cioslowski, J. and Fox, D. J.: Gaussian 16, Revision A.03, Gaussian Inc, Wallingford CT, 2016.
- Gettelman, A. and Kahn, R.: Aerosols are critical for "nowcasting" climate, One Earth, 8, 101239, http://doi.org/10.1016/j.oneear.2025.101239, 2025.
  - Halonen, R., Zapadinsky, E., Kurtén, T., Vehkamäki, H. and Reischl, B.: Rate enhancement in collisions of sulfuric acid molecules due to long-range intermolecular forces, Atmos. Chem. Phys., 19, 13355–13366, http://doi.org/10.5194/acp-19-13355-2019, 2019.
- He, X.-C., Simon, M., Iyer, S., Xie, H.-B., Rörup, B., Shen, J., Finkenzeller, H., Stolzenburg, D., Zhang, R., Baccarini, A.,
  Tham, Y. J., Wang, M., Amanatidis, S., Piedehierro, A. A., Amorim, A., Baalbaki, R., Brasseur, Z., Caudillo, L., Chu, B.,
  Dada, L., Duplissy, J., Haddad, I. E., Flagan, R. C., Granzin, M., Hansel, A., Heinritzi, M., Hofbauer, V., Jokinen, T.,
  Kemppainen, D., Kong, W., Krechmer, J., Kürten, A., Lamkaddam, H., Lopez, B., Ma, F., Mahfouz, N. G. A., Makhmutov,
  V., Manninen, H. E., Marie, G., Marten, R., Massabò, D., Mauldin, R. L., Mentler, B., Onnela, A., Petäjä, T., Pfeifer, J.,
  Philippov, M., Ranjithkumar, A., Rissanen, M. P., Schobesberger, S., Scholz, W., Schulze, B., Surdu, M., Thakur, R. C.,
- Tomé, A., Wagner, A. C., Wang, D., Wang, Y., Weber, S. K., Welti, A., Winkler, P. M., Zauner-Wieczorek, M., Baltensperger, U., Curtius, J., Kurtén, T., Worsnop, D. R., Volkamer, R., Lehtipalo, K., Kirkby, J., Donahue, N. M., Sipilä, M. and Kulmala, M.: Iodine oxoacids enhance nucleation of sulfuric acid particles in the atmosphere, Science, 382, 1308–1314, http://doi.org/10.1126/science.adh2526, 2023.
- He, X.-C., Tham, Y. J., Dada, L., Wang, M., Finkenzeller, H., Stolzenburg, D., Iyer, S., Simon, M., "rten, A. K., Shen, J.,
  Roerup, B., Rissanen, M., Schobesberger, S., Baalbaki, R., Wang, D. S., Koenig, T. K., Jokinen, T., Sarnela, N., Beck, L. J., Almeida, J., Amanatidis, S., Amorim, A., Ataei, F., Baccarini, A., Bertozzi, B., Bianchi, F., Brilke, S., Caudillo, L., Chen, D., Chiu, R., Chu, B., Dias, A., Ding, A., Dommen, J., Duplissy, J., Haddad, I. E., Carracedo, L. G., Granzin, M., Hansel, A., Heinritzi, M., Hofbauer, V., Junninen, H., Kangasluoma, J., Kemppainen, D., Kim, C., Kong, W., Krechmer, J. E., Kvashin, A., Laitinen, T., Lamkaddam, H., Lee, C. P., Lehtipalo, K., Leiminger, M., Li, Z., Makhmutov, V.,
- Manninen, H. E., Marie, G., Marten, R., Mathot, S., Mauldin, R. L., Mentler, B., Moehler, O., Mueller, T., Nie, W., Onnela, A., Petaja, T., Pfeifer, J., Philippov, M., Ranjithkumar, A., Saiz-Lopez, A., Salma, I., Scholz, W., Schuchmann, S., Schulze, B., Steiner, G., Stozhkov, Y., Tauber, C., Tome, A., Thakur, R. C., Vaisanen, O., Vazquez-Pufleau, M., Wagner, A. C., Wang, Y., Weber, S. K., Winkler, P. M., Wu, Y., Xiao, M., Yan, C., Ye, Q., Ylisirnio, A., Zauner-Wieczorek, M., Zha, Q., Zhou, P., Flagan, R. C., Curtius, J., Baltensperger, U., Kulmala, M., Kerminen, V.-M., Kurten, T., Donahue, N. M.,
  Volkemer, P., Kirkhy, L., Worsner, D. P. and Sipile, M.: Pole of inding avereids in atmospheric agreed puglection.
- Volkamer, R., Kirkby, J., Worsnop, D. R. and Sipila, M.: Role of iodine oxoacids in atmospheric aerosol nucleation, Science, 371, 589–595, http://doi.org/10.1126/science.abe0298, 2021.
  - Hodshire, A. L., Campuzano-Jost, P., Kodros, J. K., Croft, B., Nault, B. A., Schroder, J. C., Jimenez, J. L. and Pierce, J. R.: The potential role of methanesulfonic acid (MSA) in aerosol formation and growth and the associated radiative forcings, Atmos. Chem. Phys., 19, 3137–3160, http://doi.org/10.5194/acp-19-3137-2019, 2019.



455



- 440 Hoffmann, E. H., Tilgner, A., Schrödner, R., Bräuer, P., Wolke, R. and Herrmann, H.: An advanced modeling study on the impacts and atmospheric implications of multiphase dimethyl sulfide chemistry, Proc. Natl. Acad. Sci. U. S. A., 113, 11776-11781, http://doi.org/10.1073/pnas.1606320113, 2016.
  - Holzer, C., Franzke, Y. J. and Pausch, A.: Current density functional framework for spin-orbit coupling, J. Chem. Phys., 157, 204102, http://doi.org/doi.org/10.1063/5.0122394, 2022.
- Kuhn, M. and Weigend, F.: Two-component hybrid time-dependent density functional theory within the Tamm-Dancoff approximation, J. Chem. Phys., 142, 034116, http://doi.org/10.1063/1.4905829, 2015.
  - Kulmala, M., Kontkanen, J., Junninen, H., Lehtipalo, K., Manninen, H. E., Nieminen, T., Petäjä, T., Sipilä, M., Schobesberger, S., Rantala, P., Franchin, A., Jokinen, T., Järvinen, E., Äijälä, M., Kangasluoma, J., Hakala, J., Aalto, P. P., Paasonen, P., Mikkilä, J., Vanhanen, J., Aalto, J., Hakola, H., Makkonen, U., Ruuskanen, T., Mauldin, R. L., 3rd, Duplissy, J., Vehkamäki,
- H., Bäck, J., Kortelainen, A., Riipinen, I., Kurtén, T., Johnston, M. V., Smith, J. N., Ehn, M., Mentel, T. F., Lehtinen, K.
   E., Laaksonen, A., Kerminen, V. M. and Worsnop, D. R.: Direct observations of atmospheric aerosol nucleation, Science, 339, 943–946, http://doi.org/10.1126/science.1227385, 2013.
  - Lehtinen, K. E. J., Dal Maso, M., Kulmala, M. and Kerminen, V.-M.: Estimating nucleation rates from apparent particle formation rates and vice versa: Revised formulation of the Kerminen–Kulmala equation, J. Aerosol Sci., 38, 988–994, http://doi.org/10.1016/j.jaerosci.2007.06.009, 2007.
  - Lehtipalo, K., Rondo, L., Kontkanen, J., Schobesberger, S., Jokinen, T., Sarnela, N., Kürten, A., Ehrhart, S., Franchin, A., Nieminen, T., Riccobono, F., Sipilä, M., Yli-Juuti, T., Duplissy, J., Adamov, A., Ahlm, L., Almeida, J., Amorim, A., Bianchi, F., Breitenlechner, M., Dommen, J., Downard, A. J., Dunne, E. M., Flagan, R. C., Guida, R., Hakala, J., Hansel, A., Jud, W., Kangasluoma, J., Kerminen, V.-M., Keskinen, H., Kim, J., Kirkby, J., Kupc, A., Kupiainen-Määttä, O.,
- Laaksonen, A., Lawler, M. J., Leiminger, M., Mathot, S., Olenius, T., Ortega, I. K., Onnela, A., Petäjä, T., Praplan, A., Rissanen, M. P., Ruuskanen, T., Santos, F. D., Schallhart, S., Schnitzhofer, R., Simon, M., Smith, J. N., Tröstl, J., Tsagkogeorgas, G., Tomé, A., Vaattovaara, P., Vehkamäki, H., Vrtala, A. E., Wagner, P. E., Williamson, C., Wimmer, D., Winkler, P. M., Virtanen, A., Donahue, N. M., Carslaw, K. S., Baltensperger, U., Riipinen, I., Curtius, J., Worsnop, D. R. and Kulmala, M.: The effect of acid–base clustering and ions on the growth of atmospheric nano-particles, Nat. Commun., 7, 11594, http://doi.org/10.1038/ncomms11594, 2016.
  - Li, J., Ning, A., Liu, L. and Zhang, X.: Atmospheric Bases-Enhanced Iodic Acid Nucleation: Altitude-Dependent Characteristics and Molecular Mechanisms, Environ. Sci. Technol., http://doi.org/10.1021/acs.est.4c06053, 2024.
    - Li, Y., Shen, J., Zhao, B., Cai, R., Wang, S., Gao, Y., Shrivastava, M., Gao, D., Zheng, J., Kulmala, M. and Jiang, J.: A dynamic parameterization of sulfuric acid–dimethylamine nucleation and its application in three-dimensional modeling, Atmos. Chem. Phys., 23, 8789–8804, http://doi.org/10.5194/acp-23-8789-2023, 2023.
    - Liu, L., Li, S., Zu, H. and Zhang, X.: Unexpectedly significant stabilizing mechanism of iodous acid on iodic acid nucleation under different atmospheric conditions, Sci. Total Environ., 859, 159832, http://doi.org/10.1016/j.scitotenv.2022.159832, 2023.



485



- Liu, Y., Xie, H.-B., Ma, F., Chen, J. and Elm, J.: Amine-enhanced methanesulfonic acid-driven nucleation: Predictive model and cluster formation mechanism, Environ. Sci. Technol., 56, 7751–7760, http://doi.org/10.1021/acs.est.2c01639, 2022.
  - Lu, T. and Chen, F.: Multiwfn: a multifunctional wavefunction analyzer, J. Comput. Chem., 33, 580–592, http://doi.org/10.1002/jcc.22885, 2012.
  - Lu, T. and Chen, Q.: Shermo: A general code for calculating molecular thermochemistry properties, Comput. Theor. Chem., 1200, 113249, http://doi.org/10.1016/j.comptc.2021.113249, 2021.
- 480 Ma, F., Xie, H. B., Zhang, R., Su, L., Jiang, Q., Tang, W., Chen, J., Engsvang, M., Elm, J. and He, X. C.: Enhancement of atmospheric nucleation precursors on iodic acid-induced nucleation: Predictive model and mechanism, Environ. Sci. Technol., 57, 6944–6954, http://doi.org/10.1021/acs.est.3c01034, 2023.
  - McGrath, M. J., Olenius, T., Ortega, I. K., Loukonen, V., Paasonen, P., Kurtén, T., Kulmala, M. and Vehkamäki, H.: Atmospheric Cluster Dynamics Code: a flexible method for solution of the birth-death equations, Atmos. Chem. Phys., 12, 2345–2355, http://doi.org/10.5194/acp-12-2345-2012, 2012.
  - Mohd Zaki, N. H., Ali, A. M. M., Mohamad Taib, M. F., Wan Ismail, W. I. N., Sepeai, S. and Ramli, A.: Dispersion-correction density functional theory (DFT+D) and spin-orbit coupling (SOC) method into the structural, electronic, optical and mechanical properties of CH<sub>3</sub>NH<sub>3</sub>PbI<sub>3</sub>, Comput. Condens. Matte., 34, e00777, http://doi.org/10.1016/j.cocom.2022.e00777, 2023.
- 490 Neese, F.: The ORCA program system, WIREs Comput. Mol. Sci., 2, 73–78, http://doi.org/10.1002/wcms.81, 2012.
  - Ning, A., Liu, L., Ji, L. and Zhang, X.: Molecular-level nucleation mechanism of iodic acid and methanesulfonic acid, Atmos. Chem. Phys., 22, 6103–6114, http://doi.org/10.5194/acp-22-6103-2022, 2022a.
  - Ning, A., Liu, L., Zhang, S., Yu, F., Du, L., Ge, M. and Zhang, X.: The critical role of dimethylamine in the rapid formation of iodic acid particles in marine areas, npj Clim. Atmos. Sci., 5, 92, http://doi.org/10.1038/s41612-022-00316-9, 2022b.
- 495 Ning, A., Shen, J., Zhao, B., Wang, S., Cai, R., Jiang, J., Yan, C., Fu, X., Zhang, Y., Li, J., Ouyang, D., Sun, Y., Saiz-Lopez, A., Francisco, J. S. and Zhang, X.: Overlooked significance of iodic acid in new particle formation in the continental atmosphere, Proc. Natl. Acad. Sci. U. S. A., 121, e2404595121, http://doi.org/10.1073/pnas.2404595121, 2024.
  - Ning, A. and Zhang, X.: The synergistic effects of methanesulfonic acid (MSA) and methanesulfinic acid (MSIA) on marine new particle formation, Atmos. Environ., 269, 118826, http://doi.org/10.1016/j.atmosenv.2021.118826, 2022.
- 500 O'Dowd, C. D. and Leeuw, G. d.: Marine aerosol production: a review of the current knowledge, Philos. T. R. Soc. A 365, 1753–1774, http://doi.org/10.1098/rsta.2007.2043, 2007.
  - Perraud, V., Horne, J. R., Martinez, A. S., Kalinowski, J., Meinardi, S., Dawson, M. L., Wingen, L. M., Dabdub, D., Blake, D. R., Gerber, R. B. and Finlayson-Pitts, B. J.: The future of airborne sulfur-containing particles in the absence of fossil fuel sulfur dioxide emissions, Proc. Natl. Acad. Sci. U. S. A., 112, 13514–13519, http://doi.org/10.1073/pnas.1510743112, 2015.





- Peterson, K. A., Figgen, D., Goll, E., Stoll, H. and Dolg, M.: Systematically convergent basis sets with relativistic pseudopotentials. II. Small-core pseudopotentials and correlation consistent basis sets for the post-d group 16–18 elements, J. Chem. Phys., 119, 11113–11123, http://doi.org/10.1063/1.1622924, 2003.
- Quéléver, L. L. J., Dada, L., Asmi, E., Lampilahti, J., Chan, T., Ferrara, J. E., Copes, G. E., Pérez-Fogwill, G., Barreira, L.,
   Aurela, M., Worsnop, D. R., Jokinen, T. and Sipilä, M.: Investigation of new particle formation mechanisms and aerosol processes at Marambio Station, Antarctic Peninsula, Atmos. Chem. Phys., 22, 8417–8437, http://doi.org/10.5194/acp-22-8417-2022, 2022.
  - Rong, H., Liu, J., Zhang, Y., Du, L., Zhang, X. and Li, Z.: Nucleation mechanisms of iodic acid in clean and polluted coastal regions, Chemosphere, 253, 126743, http://doi.org/10.1016/j.chemosphere.2020.126743, 2020.
- Salignat, R., Rissanen, M., Iyer, S., Baray, J.-L., Tulet, P., Metzger, J.-M., Brioude, J., Sellegri, K. and Rose, C.: Measurement report: Insights into the chemical composition and origin of molecular clusters and potential precursor molecules present in the free troposphere over the southern Indian Ocean: observations from the Maïdo Observatory (2150 m a.s.l., Réunion), Atmos. Chem. Phys., 24, 3785–3812, http://doi.org/10.5194/acp-24-3785-2024, 2024.
  - Sarr, S., Graton, J., Rahali, S., Montavon, G. F. and Galland, N.: Delocalized relativistic effects, from the viewpoint of halogen bonding, Phys. Chem. Chem. Phys., 23, 4064–4074, http://doi.org/10.1039/D0CP05840H, 2021.
  - Sipilä, M., Sarnela, N., Jokinen, T., Henschel, H., Junninen, H., Kontkanen, J., Richters, S., Kangasluoma, J., Franchin, A., peräkylä, O., Rissanen, M. P., Ehn, M., Vehkamäki, H., Kurten, T., Berndt, T., Petäjä, T., Worsnop, D., Ceburnis, D., Kerminen, V. M., Kulmala, M. and O'Dowd, C.: Molecular-scale evidence of aerosol particle formation via sequential addition of HIO<sub>3</sub>, Nature, 537, 532–534, http://doi.org/10.1038/nature19314, 2016.
- Stolzenburg, D., Simon, M., Ranjithkumar, A., Kürten, A., Lehtipalo, K., Gordon, H., Ehrhart, S., Finkenzeller, H., Pichelstorfer, L., Nieminen, T., He, X.-C., Brilke, S., Xiao, M., Amorim, A., Baalbaki, R., Baccarini, A., Beck, L., Bräkling, S., Caudillo Murillo, L., Chen, D., Chu, B., Dada, L., Dias, A., Dommen, J., Duplissy, J., El Haddad, I., Fischer, L., Gonzalez Carracedo, L., Heinritzi, M., Kim, C., Koenig, T. K., Kong, W., Lamkaddam, H., Lee, C. P., Leiminger, M., Li, Z., Makhmutov, V., Manninen, H. E., Marie, G., Marten, R., Müller, T., Nie, W., Partoll, E., Petäjä, T., Pfeifer, J., Philippov,
- M., Rissanen, M. P., Rörup, B., Schobesberger, S., Schuchmann, S., Shen, J., Sipilä, M., Steiner, G., Stozhkov, Y., Tauber, C., Tham, Y. J., Tomé, A., Vazquez-Pufleau, M., Wagner, A. C., Wang, M., Wang, Y., Weber, S. K., Wimmer, D., Wlasits, P. J., Wu, Y., Ye, Q., Zauner-Wieczorek, M., Baltensperger, U., Carslaw, K. S., Curtius, J., Donahue, N. M., Flagan, R. C., Hansel, A., Kulmala, M., Lelieveld, J., Volkamer, R., Kirkby, J. and Winkler, P. M.: Enhanced growth rate of atmospheric particles from sulfuric acid, Atmos. Chem. Phys., 20, 7359–7372, http://doi.org/10.5194/acp-20-7359-2020, 2020.
  - Verstraete, M. J., Torrent, M., Jollet, F. c., Zérah, G. and Gonze, X.: Density functional perturbation theory with spin-orbit coupling: Phonon band structure of lead, Phys. Rev. B, 78, 045119, http://doi.org/10.1103/PhysRevB.78.045119, 2008.
  - Xavier, C., de Jonge, R. W., Jokinen, T., Beck, L., Sipila, M., Olenius, T. and Roldin, P.: Role of Iodine-Assisted Aerosol Particle Formation in Antarctica, Environ. Sci. Technol., 58, 7314–7324, http://doi.org/10.1021/acs.est.3c09103, 2024.





- Xia, D., Chen, J., Yu, H., Xie, H. B., Wang, Y., Wang, Z., Xu, T. and Allen, D. T.: Formation Mechanisms of Iodine-Ammonia Clusters in Polluted Coastal Areas Unveiled by Thermodynamics and Kinetic Simulations, Environ. Sci. Technol., 54, 9235–9242, http://doi.org/10.1021/acs.est.9b07476, 2020.
  - Yan, J., Jung, J., Zhang, M., Xu, S., Lin, Q., Zhao, S. and Chen, L.: Significant Underestimation of Gaseous Methanesulfonic Acid (MSA) over Southern Ocean, Environ. Sci. Technol., 53, 13064–13070, http://doi.org/10.1021/acs.est.9b05362, 2019.
- Yu, F. and Luo, G.: Modeling of gaseous methylamines in the global atmosphere: impacts of oxidation and aerosol uptake, Atmos. Chem. Phys., 14, 12455–12464, http://doi.org/10.5194/acp-14-12455-2014, 2014.
  - Zhang, R., Khalizov, A., Wang, L., Hu, M. and Xu, W.: Nucleation and growth of nanoparticles in the atmosphere, Chem. Rev., 112, 1957–2011, http://doi.org/10.1021/cr2001756, 2012.
- Zhang, R., Xie, H. B., Ma, F., Chen, J., Iyer, S., Simon, M., Heinritzi, M., Shen, J., Tham, Y. J., Kurtén, T., Worsnop, D. R.,
  Kirkby, J., Curtius, J., Sipilä, M., Kulmala, M. and He, X. C.: Critical Role of Iodous Acid in Neutral Iodine Oxoacid
  Nucleation, Environ. Sci. Technol., 56, 14166–14177, http://doi.org/10.1021/acs.est.2c04328, 2022.